Spin polarization and chiral condensation in a (2 + 1)-flavor Nambu–Jona-Lasinio model at finite temperature and baryon chemical potential

Aman Abhishek[*]

Theory Division, Physical Research Laboratory, Navrangpura, Ahmedabad 380 009, India and Indian Institute of Technology Gandhinagar, Gandhinagar 382355, Gujarat, India

Arpan Das[†] and Hiranmaya Mishra[‡]

Theory Division, Physical Research Laboratory, Navrangpura, Ahmedabad 380 009, India

Ranjita K. Mohapatra[§]

Department of Physics, Indian Institute of Technology Bombay, Powai, Mumbai 400076, India

(Received 17 May 2019; published 6 December 2019)

We investigate the ferromagnetic (spin polarization) condensation in $(2+1)$-flavor Nambu–Jona-Lasinio (NJL) model with nonzero current quark masses at finite temperature and density, which may be relevant in the context of neutron stars. The spin polarization condensation arises due to a tensor-type interaction that may be generated due to nonperturbative effects in QCD. In this investigation, we study the interplay between the chiral condensate and spin polarization condensation for different values of tensor coupling. Spin polarization in the case of $(2+1)$ flavor is different from two-flavor case because of an additional $F_8 \sim \langle \bar{\psi}\Sigma_z\lambda^8\psi\rangle$ along with a $F_3 \sim \langle \bar{\psi}\Sigma_z\lambda^3\psi\rangle$ condensate associated with the λ_8 flavor generator. We find nonzero values of the two spin condensates in the chirally restored phase. Beyond a certain temperature, the spin polarization condensates vanish for any value of quark chemical potential. The spin condensates affect the chiral phase transition, quark masses, and quark dispersion relation. Thermodynamic behaviors of F_3 and F_8 are found to be different, and they affect the quark masses differently. We discuss the phase diagram in the temperature and chemical potential plane in the presence of such condensates.

DOI: 10.1103/PhysRevD.100.114012

I. INTRODUCTION

One of the recent interests in high-energy physics is to study the phase diagram of strongly interacting matter. The QCD phase diagram has been studied extensively in the temperature (T)-baryon chemical potential (μ_B) plane [1,2]. The first principle lattice QCD (LQCD) simulations give a reliable prediction about the nature of QCD phases and phase transitions at zero baryon chemical potential and finite temperature [3–5]. Although LQCD calculations can be trusted at small baryon chemical potential $\mu_B \simeq 0$ using extrapolation, at relatively large baryon chemical potential, the "fermion sign problem" [6] in LQCD prevents one from making reliable estimates. LQCD calculations predict that at $\mu_B = 0$ the nature of the transition from the confined hadronic phase to deconfined quark gluon plasma (QGP) phase is not a thermodynamic phase transition; rather, it is a smooth crossover with a transition temperature $T_c \in [149\text{–}163]$ MeV [7]. On the other hand, QCD-inspired effective field theory models, e.g., the Nambu–Jona-Lasinio model (NJL), etc., indicate that the phase transition from the hadronic phase to the QGP phase at large baryon chemical potential and small temperature is first order in nature with physical quark masses. This indicates the presence of a critical end point at the end of the first-order chiral phase transition line in the QCD phase diagram. Apart from the confined hadronic phase and deconfined QGP phases, the QCD phase diagram has a very rich structure at a low temperature and high baryon chemical potential. In this region of the phase diagram, the possibility of various exotic phases, such as the color superconducting phase [8–10], quarkyonic phase [11], inhomogeneous chiral condensed phase [12–14], etc., has been investigated.

Heavy ion collision experiments, e.g., the Relativistic Heavy Ion Collider and LHC, give us a unique opportunity

[*]aman@prl.res.in
[†]arpan@prl.res.in
[‡]hm@prl.res.in
[§]ranjita@iitb.ac.in

to explore the QCD phase diagram. Strongly interacting QGP produced in these experiments at relativistic energies recreates the physical conditions of the microsecond-old Universe just after the big bang. The strongly interacting plasma produced in these high-energy collisions can be characterized as high-temperature and low baryon chemical potential QGP. At high densities relative to nuclear saturation density and low temperature, exotic phases of QCD can exist, e.g., the two-flavor color superconducting phase, color-flavor locked phase, crystalline color superconductor, etc. Some of these high-density QCD phases can also be explored in the upcoming heavy ion collision experiments at moderate center-of-mass energies at Facility for Antiproton and Ion Research and Nuclotron based Ion Collider fAcility. Apart from these terrestrial experiments, the interior of astrophysical ultracompact objects like neutron stars provide an ideal condition to indirectly explore these high-density QCD phases. Because of very low temperature and high baryon density, in the interior of a neutron star, various QCD phases may be realized, e.g., deconfined quark matter [15,16], meson condensation in the hadronic phase [17], the two-flavor color superconducting phase(2SC), the color-flavor locked phase (CFL) [8–10], etc.

Further, compact objects like neutron stars can be strongly magnetized. Observations indicate that the magnetic field strength at the surface of pulsars can be of the order of 10^{12}–10^{13} G [18]. Strongly magnetized neutron stars (magnetars) may have even stronger magnetic fields, approximately 10^{15}–10^{16} G [19–25]. Using the virial theorem and comparing the magnetic field energy and gravitational energy, one can estimate the physical upper bound on the strength of the magnetic field for a gravitationally bound star to be of the order 10^{18} G [18]. For self-bound objects like quark stars, this bound can be even higher [26]. The physical origin of the very strong magnetic field in the magnetars requires reconsideration of the common understanding that the magnetic field of a neutron star is originated from the progenitor star [27]. Since quark matter can be present at high densities inside the neutron stars, the presence of a quark ferromagnetic phase in high-density quark matter has also been suggested as a possible explanation of large magnetic field associated with magnetars [28–30]. For a possible solution to this problem, the author in Ref. [28] examined the possible existence of spin polarized deconfined quark matter using one-gluon-exchange interaction between quarks in Fermi liquid theory within the Hartree-Fock approximation. Taking the idea as proposed in the Ref. [28], spin polarization in the quark matter has been well explored in the subsequent literature. In general, a collective spin polarization of charged quarks can give rise to the ferromagnetic nature of quark matter at high density; hence, the spin of the fermions plays the crucial role in determining the possibility of the ferromagnetic nature of dense quark matter. It has been shown that in the nonrelativistic framework there is no possibility of spin polarization in normal nuclear matter [31]. On the contrary, using the relativistic Hartree-Fock approximation, the possibility of spin polarization at asymptotic high density has been suggested in Refs. [32,33]. It is important to note that the relativistic framework may be more suitable than the nonrelativistic approach to understanding the existence of spin polarization. But in any case, to explore spin polarization in quark matter at a high density or baryon chemical potential, a relativistic approach is very natural.

In the relativistic framework, "spin density" can be expressed in two different ways: first by the spatial component of the axial vector (AV) mean field, $\psi^\dagger\Sigma^i\psi \equiv -\bar{\psi}\gamma_5\gamma^i\psi$, constructed out of the fermionic field (quarks) ψ and an axial vector combination of Dirac gamma matrices and, second, by tensor Dirac bilinear (T) $\psi^\dagger\gamma^0\Sigma^i\psi \equiv -\bar{\psi}\sigma^{12}\psi$. Although AV- and T-type mean fields are different in the massless limit of fermions, it has been shown that they are equivalent in nonrelativistic approximation [29]. The coexistence of the spin polarization and color superconductivity has been studied using the AV interaction for quark matter in the NJL model [30]. The interplay between the spin polarization and chiral symmetry breaking at finite density for a single quark flavor using the AV mean field has also been studied within the NJL model in Ref. [34]. In Ref. [34], it has been shown that for one flavor spin polarization is possible at finite density and zero temperature, provided the ratio of the couplings of the axial vector channel and the pseudoscalar channel satisfies some lower bound. It has been argued in Ref. [34] that, due to the interplay between spin polarization and chiral symmetry for a certain value of chemical potential, spin polarization appears due to the large dynamical quark masses generated by spontaneous chiral symmetry breaking. Interestingly, it was also shown that spin polarization plays an important role in changing the value of the dynamical mass and that at a very high density both dynamical quark mass and spin polarization vanish in the chiral symmetric phase. Although in Ref. [28] the author introduced the idea of quark spin polarization using one-gluon-exchange interaction, in the NJL model studies, the AV mean field has been used. Because of the Fierz transformation, one can get AV channel interaction between quarks from one-gluon-exchange interaction, but the tensor Dirac bilinear representation of the spin density operator does not appear in the Fierz transformation of the one-gluon-exchange interaction. Hence, at asymptotically high densities at which one-gluon-exchange interaction in perturbative QCD is applicable, spin polarization cannot be studied using the T-channel interaction. But for moderate densities near the chiral phase transition density, perturbative QCD is not applicable, and one can use QCD-inspired low-energy effective models, e.g., the NJL model. The NJL model is not directly related to perturbative one-gluon-exchange interaction. In NJL model, AV- or T-channel interactions are not written keeping in mind the perturbative nature of QCD

and some nonperturbative effects can give rise to tensor channel interaction. Hence, spin polarization in the tensor channel, which can be different from the AV channel, can be studied within the NJL model. In fact, the tensor channel opens up a completely different point of view in looking into the spin polarization problem of quark matter at moderate densities, e.g., in the two-flavor NJL model, the spin polarized phase can be shown to be present in the chiral restored phase in which the dynamical quark mass is zero [35,36]. This result is different than the result obtained in Ref. [34], in which the spin polarization is not present in chiral restored phase. Since the manifestations of the AV- and T-channel interactions are different, the interplay between the AV- and T-type spin polarized phases becomes interesting to study along with the other phases expected to arise in the high baryon density region of the QCD phase diagram [12,30,34,35,37–41].

In the present work, we discuss the interplay between the spin polarization condensate ($\langle\bar{\psi}\Sigma^i\psi\rangle$) and the scalar chiral condensate ($\langle\bar{\psi}\psi\rangle$) in the $(2+1)$-flavor NJL model using only the T-type interaction for spin polarization. Most of the earlier works used some simplified approximation to study the interplay between spin polarization and other high-density phases, which includes the single-flavor NJL model [34], $SU(2)$-flavor NJL model [35,40], $SU(3)$-flavor NJL model [42] with zero current quark mass, etc. However, for a more realistic situation, one should consider the $(2+1)$-flavor NJL model with different current quark masses of strange and nonstrange quarks. Besides this, the structure of ferromagnetic condensation for the $(2+1)$-flavor NJL model is qualitatively different from that of the two-flavor NJL model as inherently two different kinds of spin polarizations that are associated with the diagonal generators of the $SU(3)$-flavor group are possible. The behavior of these spin polarization condensates as a function of temperature and quark chemical potential (μ) has been discussed extensively. Since the spin polarization condensates are also related to the quark-antiquark scalar condensates, it is evident that the spin polarization condensates affect the constituent mass of the quarks. In this work, spin polarization condensates due to the tensor-type interaction appear in the chiral symmetry restored phase, and the quark masses, specifically strange quark masses, are strongly affected by the spin polarization condensates in the chiral symmetric phase.

This paper is organized in the following manner. We first discuss the formalism of $(2+1)$-flavor NJL model in the presence of tensor-type interactions in Sec. II. In Sec. II, the derivation of the thermodynamic potential is discussed in a mean field approach. Once the thermodynamic potential is derived, one can get the gap equations to solve for the condensates. After the formalism, important results and the corresponding discussion are given in Sec. III. Finally, in Sec. IV, we summarize our work.

II. FORMALISM

To study the spin polarization due to tensor channel interaction for $(2+1)$ flavor quark matter, we start with the NJL Lagrangian density [39,43]

$$\mathcal{L} = \bar{\psi}(i\partial\!\!\!/ - \hat{m})\psi + \mathcal{L}_{\rm sym} + \mathcal{L}_{\rm det} + \mathcal{L}_{\rm tensor} + \mu\bar{\psi}\gamma^0\psi, \quad (1)$$

where $\psi = (u, d, s)^T$ is the three-flavor quark field and the diagonal current quark matrix is $\hat{m} = \mathrm{diag}_f(m_u, m_d, m_s)$. In this work, we have assumed that, due to isospin symmetry in the nonstrange quark sector, $m_u = m_d$. Strange quark mass m_s is different from the other light quark masses. The difference between the strange and nonstrange quark masses explicitly breaks the $SU(3)$ flavor symmetry. μ is the quark chemical potential. In the literature, different chemical potentials for the strange and nonstrange quarks have been considered, but the phase diagram has no qualitative difference. In this case, we are assuming that the quark chemical potentials of the strange and nonstrange quarks are same. Following the representations of different interaction terms as given in Ref. [43], in general, one considers

$$\mathcal{L}_{\rm sym} = g\sum_{a=0}^{a=8}[(\bar{\psi}\lambda_a\psi)^2 + (\bar{\psi}i\gamma_5\lambda_a\psi)^2]. \quad (2)$$

This term has been constructed by keeping in mind the $U(3)_L \times U(3)_R$ chiral symmetry for the three-flavor case, and it can be generalized to any number of flavors N_f. The interaction term $\mathcal{L}_{\rm sym}$ represents the four-point interaction, where $\lambda_0 = \sqrt{2/3}I_f$ and λ_a, $a = 1, \ldots (N_f^2 - 1)$ are the generators of $SU(N_f)$. In the present case I_f is the 3×3 identity matrix, and λ_a for $a = 1, \ldots 8$ are the Gell-Mann matrices.

The interaction term $\mathcal{L}_{\rm det}$ in Eq. (1) is the 't Hooft determinant interaction term. This term breaks $U(1)$ axial symmetry explicitly and also successfully describes the nonet meson properties [44–46]. It can be expressed as

$$\mathcal{L}_{\rm det} = -K\mathrm{det}_f[\bar{\psi}(1+\gamma_5)\psi + \mathrm{H.c.}]. \quad (3)$$

In this interaction term, the determinant is taken in the flavor space. This term represents the maximally flavor-mixing $2N_f$-point interaction for N_f quark flavors. For the two-flavor NJL model, this term does not introduce any new dynamics because for the two-flavor case it gives four Fermi interaction, which is already there. But for three or more flavors, this term generates a new type of interaction; e.g., for the three-flavor case, it gives rise to a six-point interaction term. The tensor interaction that is responsible for spin polarization is given as [39,42]

$$\mathcal{L}_{\text{tensor}} = \frac{G_T}{2}\sum_{a=3,8}(\bar{\psi}\Sigma_z\lambda_a\psi)^2, \quad \Sigma_z = \begin{pmatrix}\sigma_z & 0\\ 0 & \sigma_z\end{pmatrix}, \quad (4)$$

where σ_z is the third Pauli matrix. Here, we have assumed polarization along the z axis. Note that $\mathcal{L}_{\text{tensor}}$ is not invariant under chiral symmetry; rather, one requires adding a similar term with the γ^5 matrix to make the tensor interaction symmetric under chiral symmetry. Since we are not considering any condensation involving γ^5, we have omitted the term that ensures chiral invariance for the tensor interaction. Thus, the total Lagrangian with finite chemical potential becomes

$$\begin{aligned}\mathcal{L} = {}& \bar{\psi}(i\partial\!\!\!/ - \hat{m})\psi + g\sum_{a=0}^{a=8}(\bar{\psi}\lambda_a\psi)^2 \\ & - K\det{}_f[\bar{\psi}(1+\gamma_5)\psi + \text{H.c.}] \\ & + \sum_{a=3,8}\frac{G_T}{2}(\bar{\psi}\Sigma_z\lambda_a\psi)^2 + \mu\bar{\psi}\gamma^0\psi. \end{aligned} \quad (5)$$

In the mean field approximation, expanding the operators around their expectation values and neglecting higher order fluctuations, we obtain

$$\begin{aligned}(\bar{u}u)^2 &\simeq 2\langle\bar{u}u\rangle\bar{u}u - \langle\bar{u}u\rangle^2 = 2\sigma_{ud}\bar{u}u - \sigma_{ud}^2\\ (\bar{d}d)^2 &\simeq 2\langle\bar{d}d\rangle\bar{d}d - \langle\bar{d}d\rangle^2 = 2\sigma_{ud}\bar{d}d - \sigma_{ud}^2\\ (\bar{s}s)^2 &\simeq 2\langle\bar{s}s\rangle\bar{s}s - \langle\bar{s}s\rangle^2 = 2\sigma_s\bar{s}s - \sigma_s^2\\ (\bar{\psi}\Sigma_z\lambda_3\psi)^2 &\simeq 2\langle\bar{\psi}\Sigma_z\lambda_3\psi\rangle(\bar{\psi}\Sigma_z\lambda_3\psi) - \langle\bar{\psi}\Sigma_z\lambda_3\psi\rangle^2 = 2F_3(\bar{\psi}\Sigma_z\lambda_3\psi) - F_3^2\\ (\bar{\psi}\Sigma_z\lambda_8\psi)^2 &\simeq 2\langle\bar{\psi}\Sigma_z\lambda_8\psi\rangle(\bar{\psi}\Sigma_z\lambda_8\psi) - \langle\bar{\psi}\Sigma_z\lambda_8\psi\rangle^2 = 2F_8(\bar{\psi}\Sigma_z\lambda_8\psi) - F_8^2, \end{aligned} \quad (6)$$

where the chiral condensates or the quark-antiquark condensates are $\langle\bar{u}u\rangle = \langle\bar{d}d\rangle \equiv \sigma_{ud}$ and $\langle\bar{s}s\rangle \equiv \sigma_s$ and the spin polarization condensates are $F_3 = \langle\bar{\psi}\Sigma_z\lambda_3\psi\rangle$ and $F_8 = \langle\bar{\psi}\Sigma_z\lambda_8\psi\rangle$. We can write the mean field Lagrangian as

$$\mathcal{L} = \bar{\psi}(i\partial\!\!\!/ - \hat{M} + G_T F_3\Sigma_z\lambda_3 + G_T F_8\Sigma_z\lambda_8 + \mu\gamma^0)\psi - 2g(\sigma_{ud}^2 + \sigma_{ud}^2 + \sigma_s^2) + 4K\sigma_{ud}^2\sigma_s - \frac{G_T}{2}F_3^2 - \frac{G_T}{2}F_8^2, \quad (7)$$

where $\hat{M} \equiv \text{diag}(M_u, M_d, M_s)$, with effective masses,

$$\begin{aligned}M_u &= m_u - 4g\sigma_{ud} + 2K\sigma_{ud}\sigma_s\\ M_d &= m_d - 4g\sigma_{ud} + 2K\sigma_{ud}\sigma_s\\ M_s &= m_s - 4g\sigma_s + 2K\sigma_{ud}^2. \end{aligned} \quad (8)$$

For a given system at finite temperature and finite chemical potential, the most important quantity for the understanding of the thermodynamic behavior or the phase structure is the thermodynamic potential. Once the thermodynamic potential for this model is known, thermodynamic quantities can be extracted using Maxwell relations. The thermodynamic potential for the Lagrangian as given in Eq. (7) in the grand canonical ensemble at a finite temperature and finite chemical potential can be given as

$$\begin{aligned}\Omega(T,\mu,\sigma_{ud},\sigma_s,F_3,F_8) = {}& -N_c\sum_{f=u,d,s}\int\frac{d^3p}{(2\pi)^3}[(E_{f+}+E_{f-}) + T\ln(1+e^{-\beta(E_{f+}-\mu)}) + T\ln(1+e^{-\beta(E_{f+}+\mu)})\\ & + T\ln(1+e^{-\beta(E_{f-}-\mu)}) + T\ln(1+e^{-\beta(E_{f-}+\mu)})] + 2g(\sigma_{ud}^2+\sigma_{ud}^2+\sigma_s^2) - 4K\sigma_{ud}^2\sigma_s + \frac{G_T}{2}F_3^2 + \frac{G_T}{2}F_8^2,\\ = {}& -\frac{6}{4\pi^2}\sum_{f=u,d,s}\int_0^\Lambda dp_T\int_0^{\sqrt{\Lambda^2-p_T^2}}p_T dp_z[(E_{f+}+E_{f-}) + T\ln(1+e^{-\beta(E_{f+}-\mu)})\\ & + T\ln(1+e^{-\beta(E_{f+}+\mu)}) + T\ln(1+e^{-\beta(E_{f-}-\mu)}) + T\ln(1+e^{-\beta(E_{f-}+\mu)})] + 2g(\sigma_{ud}^2+\sigma_{ud}^2+\sigma_s^2)\\ & - 4K\sigma_{ud}^2\sigma_s + \frac{G_T}{2}F_3^2 + \frac{G_T}{2}F_8^2, \end{aligned} \quad (9)$$

where $N_c = 3$ is the number of colors, transverse momentum $p_T = \sqrt{p_x^2 + p_y^2}$, and the single-particle energies are

$$E_{u+} = \sqrt{p_z^2 + \left(\sqrt{p_T^2 + M_u^2} + G_T\left(F_3 + \frac{F_8}{\sqrt{3}}\right)\right)^2}$$
$$E_{u-} = \sqrt{p_z^2 + \left(\sqrt{p_T^2 + M_u^2} - G_T\left(F_3 + \frac{F_8}{\sqrt{3}}\right)\right)^2}$$
$$E_{d+} = \sqrt{p_z^2 + \left(\sqrt{p_T^2 + M_d^2} + G_T\left(F_3 - \frac{F_8}{\sqrt{3}}\right)\right)^2}$$
$$E_{d-} = \sqrt{p_z^2 + \left(\sqrt{p_T^2 + M_d^2} - G_T\left(F_3 - \frac{F_8}{\sqrt{3}}\right)\right)^2}$$
$$E_{s+} = \sqrt{p_z^2 + \left(\sqrt{p_T^2 + M_s^2} + G_T\frac{2F_8}{\sqrt{3}}\right)^2}$$
$$E_{s-} = \sqrt{p_z^2 + \left(\sqrt{p_T^2 + M_s^2} - G_T\frac{2F_8}{\sqrt{3}}\right)^2}. \quad (10)$$

The thermodynamic behavior of the condensates can be found by solving the gap equations, which can be found from the stationary conditions (for details, see the Appendix),

$$\frac{\partial\Omega}{\partial\sigma_{ud}} = \frac{\partial\Omega}{\partial\sigma_s} = \frac{\partial\Omega}{\partial F_3} = \frac{\partial\Omega}{\partial F_8} = 0. \quad (11)$$

Gap equations can have several roots, but the solution with the lowest value of thermodynamic potential is taken as the stable solution.

The NJL model Lagrangian in $(3+1)$ dimensions has operators that have mass dimension more than 4; thus, it can shown to be a nonrenormalizable theory [47]. Thus, the divergence coming from the 3-momentum integral of the vacuum part cannot be removed by the renormalization prescriptions. The model predictions inevitably depend on the regularization procedures, and the parameter dependence in each regularization method has been reported in Refs. [48,49]. In this work, we have considered the most frequently used three-dimensional (3D) momentum cutoff regulation scheme to regularize the divergence in Eq. (9) for thermodynamic potential.

In the study of spin polarization in the NJL model, the parameter that plays the crucial role is the tensor channel interaction G_T. If one considers only vector current interaction, e.g., one-gluon-exchange interaction in perturbative QCD processes, then such a tensor interaction cannot be generated by Fierz transformation. However, such a tensor interaction can be generated from two-gluon-exchange diagrams [39]. It is relevant to point out that one can also get tensor channel interaction by Fierz transformation from scalar and pseudoscalar interaction [35],

$$g[(\bar{\psi}\psi)^2 + (\bar{\psi}i\gamma_5\lambda_a\psi)^2] = \frac{g}{4}\left[(\bar{\psi}\psi)^2 - \frac{1}{2}(\bar{\psi}\gamma^\mu\gamma^\nu\lambda_a\psi)^2 + \ldots..\right], \quad (12)$$

which gives $|g/G_T| = 2$. In the present investigation, we can take G_T as a free parameter to study the inter-relationship between scalar and tensor condensates. It may also be noted that the parameters g and G_T may be considered independently to derive mesonic properties [50–52]. It has been shown that the $SU(2)$ NJL model with both positive and negative tensor couplings can describe the phenomenology of mesons. Indeed, the $SU(2)$ Lagrangian has been considered with vector, axial vector, and tensor interaction in Ref. [52], in which the gap equations are solved in the usual Hartree approximation while mesons are described in the random phase approximation [52]. In this work, we have only considered G_T as a free parameter with positive values only; i.e., G_T and g are of same sign. In the literature various values have been considered, e.g., $G_T = 2g$, $1.5g$ [39] as well as $G_T = 4.0g$ [52]. We have also obtained our results by taking different values of G_T. Results with some specific parameter sets have been mentioned in Sec. III.

III. RESULTS AND DISCUSSIONS

We begin the discussion with the parametrization of the model. The parameters to be fixed are the three current quark masses (m_u, m_d, m_s), the scalar coupling (g), the determinant coupling (K), the tensor coupling (G_T), and the 3-momentum cutoff (Λ) to regularize divergent integrals. Except for the tensor coupling G_T, there are several parameter sets available for the NJL model [43]. These fits are obtained using low-energy hadronic properties such as the pion decay constant and masses of the pion, kaon, and η' [45,53,54]. The determinant interaction is important as it breaks $U(1)_A$ symmetry and gives the correct η mass. One may note that there is a discrepancy in determination of the determinant coupling K. For example, in Ref. [45], the value of the coupling differs by as much as 30% compared to the value used in present work. This discrepancy arises due to difference in the treatment of η' mesons with a high mass [43]. In fact, this leads to a nonphysical imaginary part for the corresponding polarization diagram in the η' meson channel. This is unavoidable because NJL is not confining and is unrealistic in this context. Within the above-mentioned limitations of the model and the uncertainty in the value of the determinant coupling, we proceed with the present parameter set as given in Table I [43].

Let us first note that there are four condensates, σ_{ud}, σ_s, $F_3 \equiv \langle\bar{u}\Sigma_z u\rangle - \langle\bar{d}\Sigma_z d\rangle$ and $F_8 \equiv \frac{1}{\sqrt{3}}(\langle\bar{u}\Sigma_z u\rangle + \langle\bar{d}\Sigma_z d\rangle - 2\langle\bar{s}\Sigma_z s\rangle)$, to be determined from the solution of the gap equation (11). In this context, a comment regarding neutron star matter (NSM) may be relevant. For NSM, we also need to impose the charge neutrality condition for the bulk matter. In that case, one has to solve the gap equations (11) with the constraints imposed by the charged neutrality condition. In the present investigation, however, we will explore the existence of possible spin polarization condensates at high densities without imposing the charge

TABLE I. Parameter set considered in this work for the $(2+1)$ NJL model apart from the tensor coupling G_T.

Parameter set	
Parameters and couplings	Value
3-momentum cutoff (Λ)	$\Lambda = 602.3 \times 10^{-3}$ GeV
u quark mass (m_u)	$m_u = 5.5 \times 10^{-3}$ GeV
d quark mass (m_d)	$m_d = 5.5 \times 10^{-3}$ GeV
s quark mass (m_s)	$m_s = 140.7 \times 10^{-3}$ GeV
Scalar coupling (g)	$g = 1.835/\Lambda^2$
Determinant interaction (K)	$K = 12.36/\Lambda^5$

neutrality condition similarly to Refs. [35,42] but with masses of quarks calculated self-consistently. Further, for simplicity, we shall first consider $F_8 = \frac{F_3}{\sqrt{3}}$ so that the spin polarization condensates for d quarks and s quarks are treated on the same footing, i.e., $\langle \bar{d}\Sigma_z d\rangle \equiv \langle \bar{s}\Sigma_z s\rangle$ [42]. The results in such a scenario are described below.

A. Results with $F_8 = \frac{F_3}{\sqrt{3}}$

1. Chiral phase transition and the behavior of quark masses for $G_T = 2g$ at zero temperature

Let us consider the thermodynamic potential at zero temperature as a function of quark chemical potential (μ) along with the condition $F_8 = F_3/\sqrt{3}$ [42]. In Ref. [42], the authors have taken $m_u = m_d = m_s = 0$ and considered $F_8 = F_3/\sqrt{3}$. It is important to note that for $m_u = m_d = m_s = 0$ and $F_8 = F_3/\sqrt{3}$ single- particle energies of the d quark and s quark are the same and hence d and s quarks can be considered on equal footing. This assumption is a simplification of a more general physical situation. Note that F_3 is associated with nonstrange quarks while F_8 is associated with strange and nonstrange quarks. In a more general situation, F_3 and F_8 can be independent and will be shown in this work later. However, we also consider $F_8 = F_3/\sqrt{3}$ for a comparative and qualitative study with the already existing result, e.g., in Ref. [42]. For quantitative analysis, we consider the tensor coupling $G_T = 2g$. Figure 1 shows the behavior of the constituent quark masses as a function of quark chemical potential at zero temperature in the presence as well as in the absence of spin polarization condensate F_3.

From Fig. 1, it is clear that the vacuum masses ($T = 0$, $\mu = 0$) for the nonstrange quarks are 0.368 GeV and the strange quark mass is 0.549 GeV. The vacuum masses for the constituent quarks remain the same as the case with $G_T = 0$, as the tensor condensates appear only at large chemical potential. This is the chiral symmetry broken phase in which constituent quark masses are generated dynamically. Close to $\mu = \mu_c = 0.360$ GeV, there is sudden drop in the masses of u and d quarks $M_u = M_d$. Because of the flavor mixing due to the determinant interaction, the strange quark mass also reduces at $\mu = \mu_c$ to a value approximately 460 MeV.

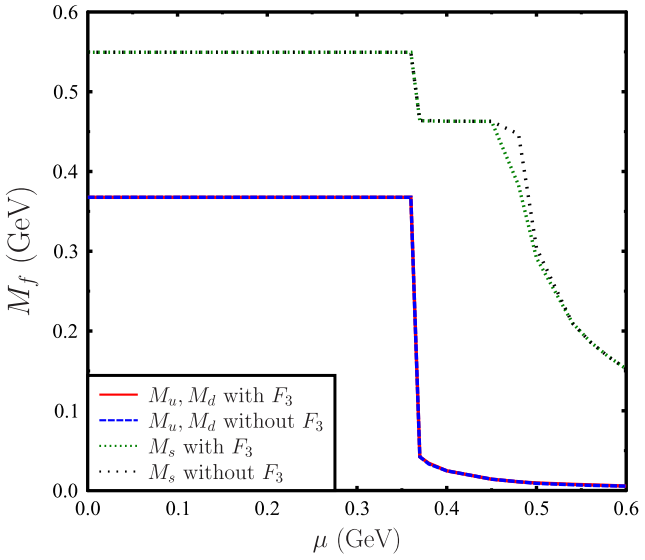

FIG. 1. Constituent quark mass as a function of quark chemical potential at zero temperature in the presence and absence of spin polarization condensation. The red solid line and green dotted line represent nonstrange and strange quark masses in the presence of spin polarization condensate F_3. The blue dashed line and black dotted line represent nonstrange and strange quark constituent masses in the standard $(2+1)$-flavor NJL model in the absence of any spin polarization condensate. A sharp jump in the value of M_u and M_s near $\mu = 0.360$ GeV indicates the first-order chiral phase transition. In this case, we have considered the tensor interaction coupling to be $G_T = 2g$. Comparing the green and black lines for the strange quark, it is clear that a nonzero value of the spin condensate affects the strange quark mass. However, the nonstrange quark masses are almost unaffected due to the presence of the spin polarization condensate. For $G_T = 2g$, a nonzero value of F_3 appears only near 0.480 GeV, which is away from the chiral phase transition critical chemical potential; hence, in this case, the chiral phase transition is unaffected by the presence of spin polarization.

This sudden change in the constituent mass indicates a first-order phase transition. It is also expected that chiral phase transition should occur in the $(2+1)$ flavor NJL model near $\mu = 0.360$ GeV at zero temperature in the absence of spin polarization. Using the gap equations, it can be shown that at zero temperature and zero chemical potential $F_3 = 0$ is a solution. It turns out that at zero temperature and zero chemical potential $F_3 = 0$ is also a stable solution, and hence F_3 does not affect the constituent quark masses at low chemical potential at zero temperature.

We can also understand the behavior of the constituent quark masses $M_u = M_d$ and M_s in the presence and absence of the spin polarization condensation by looking into the behavior of thermodynamic potential as a function of quark-antiquark condensates σ_{ud} and σ_s and spin polarization condensate F_3 for different values of temperature T and chemical potential μ. Contour plots of thermodynamic potential in the $\sigma_{ud} - \sigma_s$ plane for different values of chemical potential μ at zero temperature have been shown

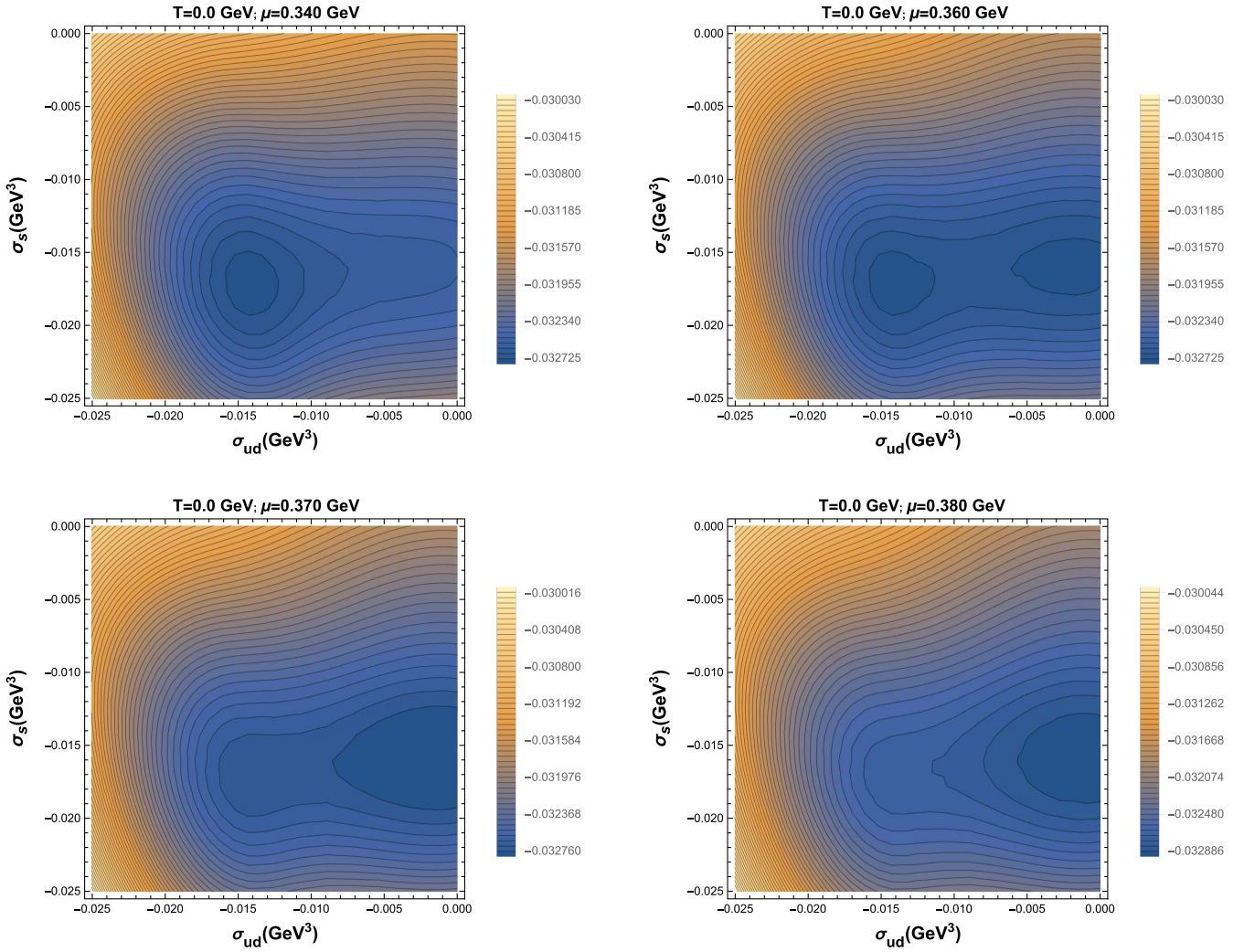

FIG. 2. The figure shows the contour maps of the thermodynamics potential with the set of parameters in Table I and $G_T = 2g$ at $T = 0.0$ GeV for different values of μ. The darker region in the plots shows the lower value of the thermodynamic potential. The horizontal and vertical axes represents the nonstrange quark condensate σ_{ud} and strange quark condensate σ_s, respectively. The existence of an almost degenerate vacuum is clear from the figure near $\mu = 0.360$ GeV. Hence, the chiral phase transition near $\mu = 0.360$ is a first-order phase transition. Spin polarization condensation F_3 has no effect on the chiral phase transition. As we have shown in Fig. 3, a nonzero value of F_3 occurs near $\mu = 0.480$ GeV at $T = 0.0$ GeV for $G_T = 2g$, which is far away from the critical quark chemical potential for the chiral phase transition.

in Fig. 2 with the set of parameters given in Table I and $G_T = 2g$. The darker regions in the plots show the lower value of the thermodynamic potential. The horizontal and vertical axes represent the nonstrange quark-antiquark condensate σ_{ud} and strange quark-antiquark condensate σ_s. As may be observed in Fig. 2, for zero temperature and $\mu < \mu_c \sim 0.360$ GeV, minimization of the thermodynamic potential gives us a unique nonzero value of the quark-antiquark condensate. This nonzero value of both σ_{ud} and σ_s indicates the chiral symmetry broken phase at zero temperature and $\mu \leq 0.360$ GeV. At $\mu = 0.360$ GeV, one can see the existence of almost degenerate vacua in the thermodynamic potential, one for $\sigma_{ud} \sim -0.015$ GeV^3 and the other at $\sigma_{ud} \sim 0.0$ GeV^3. As the chemical potential is increased, this degeneracy is lifted, and the vacuum with σ_{ud} close to zero has the minimum value for the thermodynamic potential. At $\mu = 0.4$ GeV, the value of σ_{ud} as well as M_u is very small and is close to the current quark mass value. This indicates that at chemical potential larger than $\mu_c = 0.360$ GeV chiral symmetry is restored. One may note that this restoration of chiral symmetry is partial in nature. Since current quark masses of up and down quarks are nonzero, the scalar condensate σ_{ud} is not exactly zero and hence chiral symmetry is only approximate. Also the strange quark constituent and current masses are large, as seen in Figs. 1 and 2, and break chiral symmetry for all values of quark chemical potential. As μ is further increased beyond μ_c, σ_s also approaches its (approximate) chiral limit continuously. Degeneracy in the thermodynamic potential and a sharp jump in the order parameter (σ_{ud}) indicate a first-order

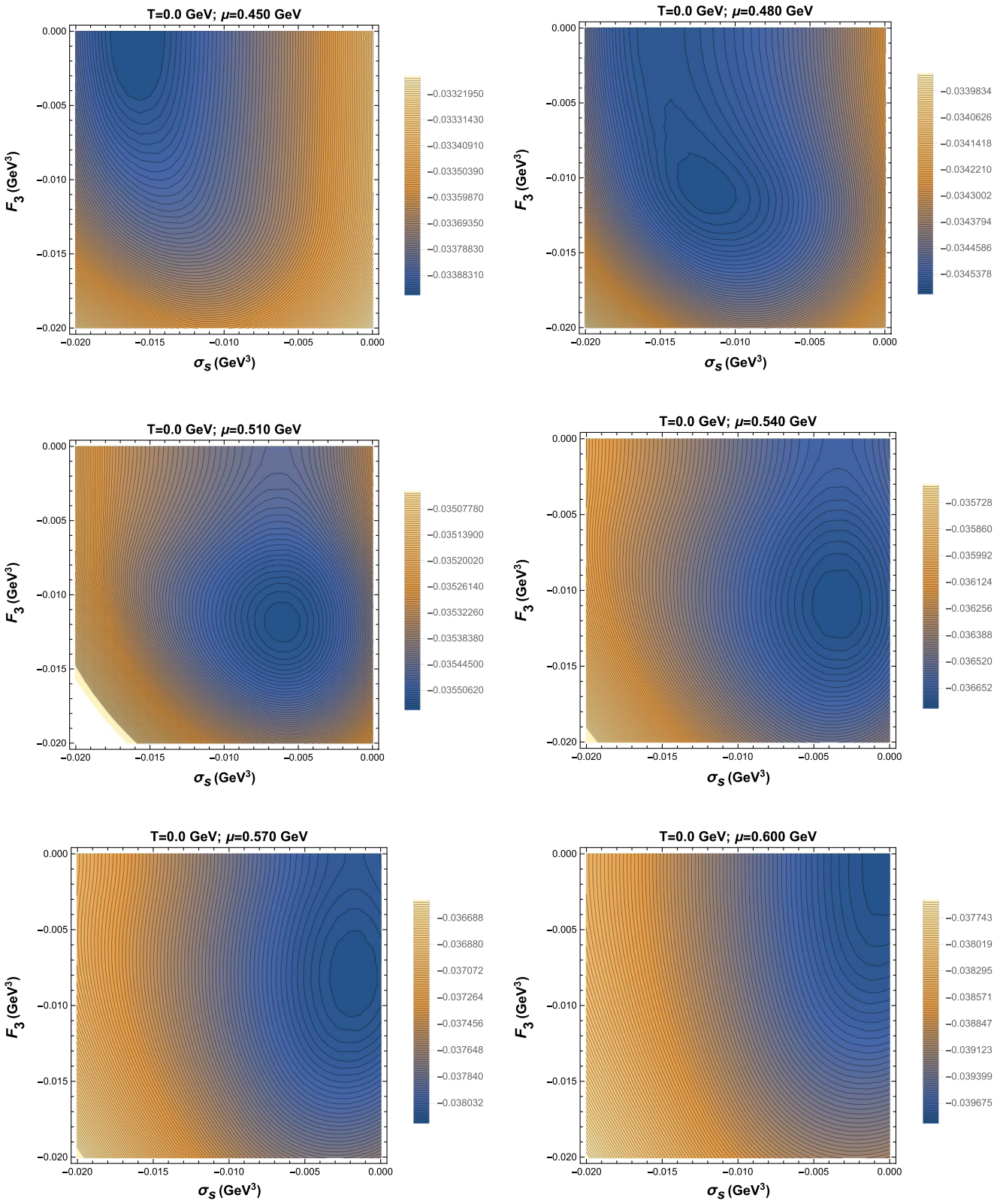

FIG. 3. This figure shows the contour plots of the thermodynamic potential in the $\sigma_s - F_3$ plane at zero temperature with different values of quark chemical potentials (μ) for the case of $G_T = 2g$ and $F_8 = F_3/\sqrt{3}$. It is clear from the plots that nonzero spin polarization appears at $\mu = 0.480$ GeV, reaches its maximum value near $\mu = 0.510$ GeV, and completely melts near $\mu = 0.600$ GeV.

phase transition. Hence, the chiral transition at zero temperature is of first order in nature. Up to μ_c, the quark number densities remain vanishing. Beyond μ_c, the number densities of light quarks become nonvanishing. The strange quark mass starts decreasing with μ beyond $\mu \sim 460$ MeV, and the strange quark density becomes nonvanishing beyond this. This first-order nature of the chiral phase transition can also be seen at finite temperature; however, at relatively larger temperature, the chiral phase transition does not remain as a first-order phase transition. In fact, the end of the first-order transition to the crossover defines the critical end point. At higher temperatures, beyond the critical temperature, the quark-antiquark condensate changes smoothly across the critical chemical potential.

As the chemical potential is increased beyond the chiral restoration for the light quarks, it is observed that the spin polarized condensate develops for a range of chemical potential. In particular, as shown in Fig. 3 for zero temperature, a nonzero F_3 starts to develop at $\mu \simeq 0.480$ GeV and increases slightly with μ, becoming a maximum around $\mu \simeq 0.510$ GeV, beyond which it decreases and eventually vanishes at $\mu \simeq 0.600$ GeV. Therefore, we observe here in Fig. 1 that the chiral transition for the light quarks is not affected by the spin polarization condensates as the latter exist at μ larger than μ_c for $G_T = 2g$. It is important to mention that both $\bar{\psi}\psi$ and $\bar{\psi}\gamma^\mu\gamma^\nu\psi$ break the chiral symmetry, but their thermodynamic behavior is quite opposite. At zero temperature and zero chemical potential, a nonzero value of scalar condensation is thermodynamically stable, while the tensor condensate vanishes. However, at high chemical potential when the tensor condensate takes a nonzero value, the chiral condensate vanishes but for small current quark mass. The noninvariance of the tensor interaction under chiral symmetry can be manifested in the change of quark masses even if the scalar condensate vanishes for the light quarks.

When we take $G_T = 2g$, the value of F_3 is not large enough near $\mu = 0.360$ GeV, and the chiral phase transition is unaffected by the spin polarization. Since quark-antiquark condensates σ_{ud} and σ_s are intimately connected with the F_3, a nonzero value of F_3 can change the quark dynamical mass (see Fig. 1). Strange quark mass is more affected by the presence of the spin polarization condensate (F_3) because the dynamical mass of the u quark becomes very small just after the chiral phase transition; however, the strange quark has a substantial mass even after the chiral phase transition. Similar to the result at zero temperature, for $G_T = 2g$, the chiral phase transition is almost unaffected in the presence of spin polarization at finite temperature also.

2. Behavior of F_3 for $G_T = 2g$

Next, let us focus our attention to the thermodynamic behavior of F_3. Figure 3 shows the contour plots of the thermodynamic potential in the $\sigma_s - F_3$ plane at zero temperature with an increasing value of the chemical potential (μ) for $G_T = 2g$. As before, the darkest regions in the contour plots show the global minimum of the thermodynamic potential, and the corresponding values of σ_s and F_3 are the correct condensation value. It is clear from the Fig. 3 that spin polarization is possible within the small range of chemical potential $\mu \simeq 0.480$–0.570 GeV at zero temperature. From this figure, it is clear that with an increase in chemical potential σ_s decreases. In this work, we have kept the value of $\mu \leq \Lambda$ because Λ is the cutoff of the theory. When the chemical potential is close to 0.6 GeV, both σ_s and F_3

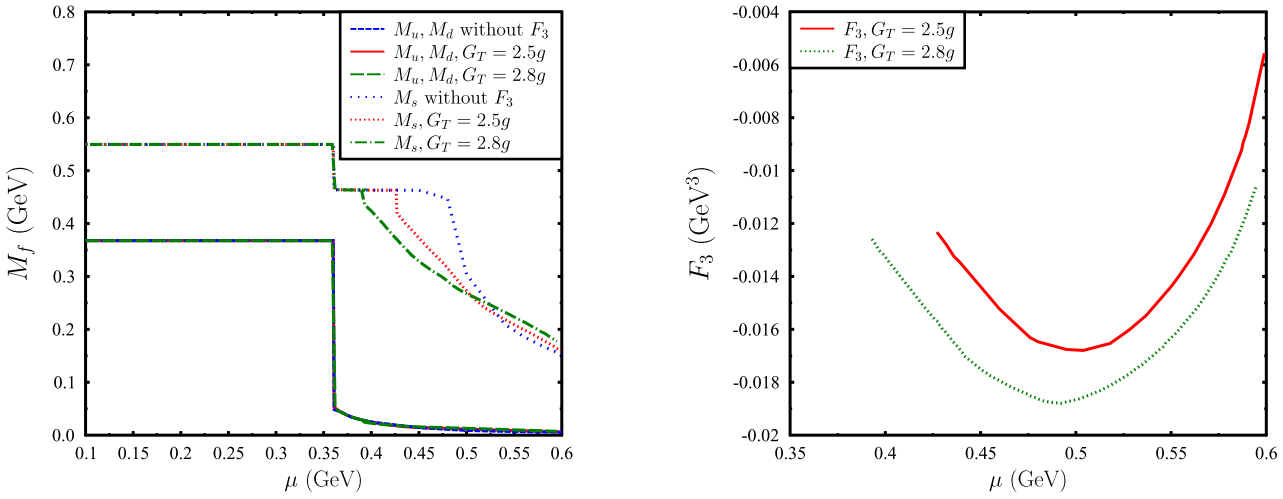

FIG. 4. Left plot: Dependence of constituent quark mass on the quark chemical potential at zero temperature in the presence as well as in the absence of spin polarization condensation for different values of tensor couplings for $F_8 = F_3/\sqrt{3}$. A sharp jump in the value of M_u and M_s near $\mu = 0.360$ GeV in both plots indicates the first-order chiral phase transition, which is expected for standard $(2+1)$-flavor NJL model. Right plot: Variation of the spin polarization condensate with quark chemical potential at zero temperature with different values of tensor couplings $G_T = 2.5g$ and $G_T = 2.8g$. For larger tensor coupling, the tensor condensate forms at relatively smaller chemical potential, and it remains nonzero for a wide range of chemical potential.

become zero. For large chemical potentials($\mu > 570$ MeV), spin polarization condensate completely melts along with the other condensates. The presence of spin polarization condensation can affect the QCD phase diagram in many different ways. As we have already mentioned that the spin polarization condensate coming from the tensor interaction also breaks the chiral symmetry, an obvious effect of a large value of spin polarization condensate should be seen in the chiral phase transition. We have also observed that F_3 decreases with increasing temperature and vanishes at a few tens of MeV. Therefore such condensates do not affect the critical end point.

3. Quark masses and ferromagnetic condensate for larger tensor coupling

The left plot and the right plot in Fig. 4 are for quark masses and the ferromagnetic condensate, respectively, for the tensor coupling $G_T = 2.5g$ and $G_T = 2.8g$. One may note that for larger tensor coupling the u and d quark masses are

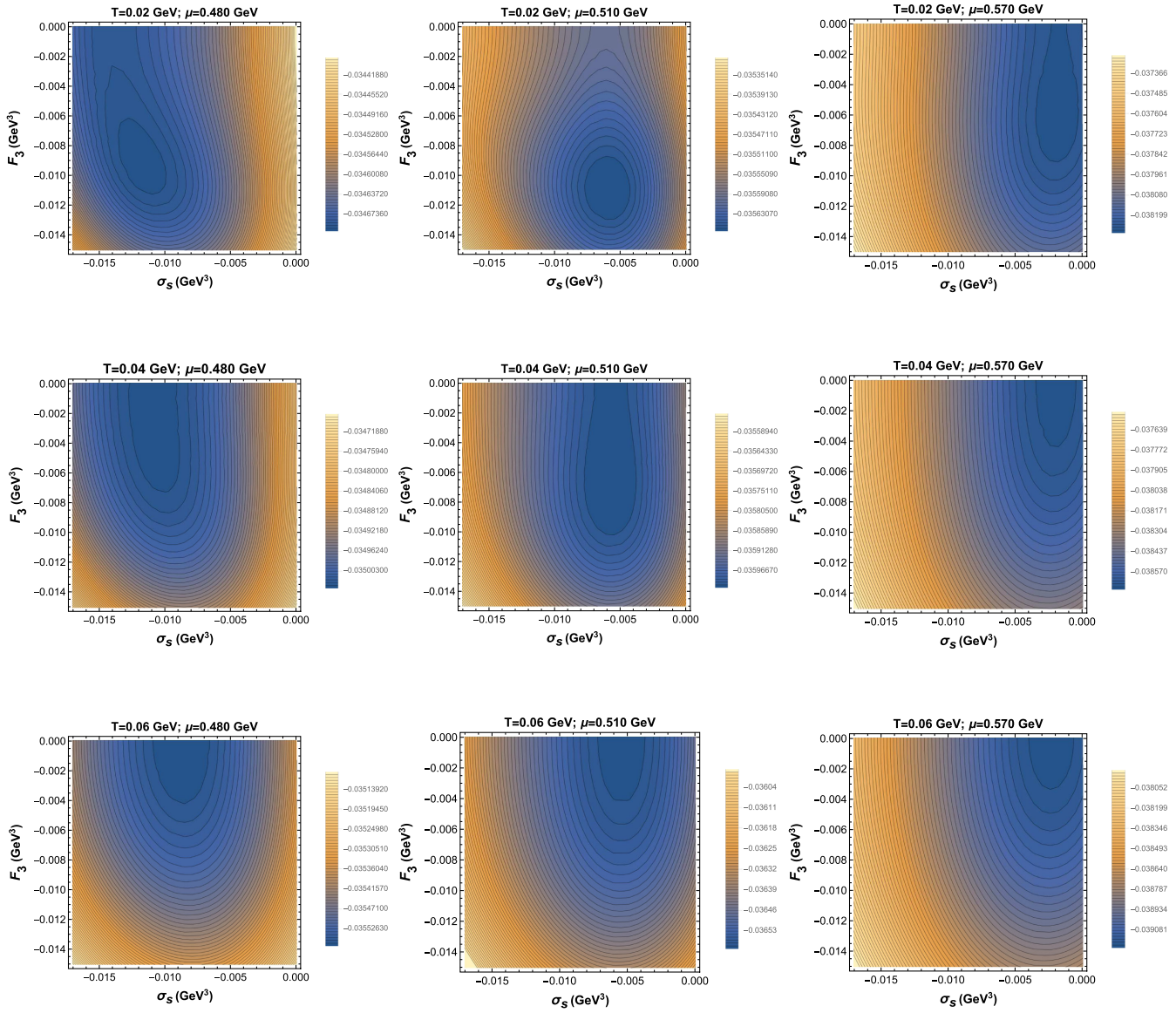

FIG. 5. This figure shows the contour plots of the thermodynamic potential in the $\sigma_s - F_3$ plane for finite temperature (T) and finite chemical potential (μ) with $G_T = 2g$ and $F_8 = F_3/\sqrt{3}$. Along each row as we move from left to the right, temperature has been kept fixed, but μ is increasing; similarly, along each column, μ has been kept fixed with T increasing. Darker regions in these contour plots show the global minimum of the thermodynamic potential. It is clear from the plots that at small temperature a nonzero value of the spin polarization starts to appear at a smaller value of the chemical potential and it also melts at higher chemical potential. Thus, for smaller temperature, the domain of μ where one can get nonzero spin polarization is larger. This domain of existence for the spin polarization condensate becomes smaller with increasing temperature T for a given value of G_T. In fact, when the temperature is $T = 0.06$ GeV, we cannot get spin polarization for any value of μ.

not affected but the strange quark mass is significantly affected. The ferromagnetic condensate is stronger for a larger value of tensor coupling and survives for a longer range of quark chemical potential. It is important to mention that for tensor couplings greater than $G_T = 3g$ the chiral transition itself is affected. However, the requirement of baryon matter stability places a upper bound on the value of tensor coupling.

4. Finite temperature effect on the spin polarization condensate F_3 for $G_T = 2g$

After demonstrating the behavior of the spin polarization condensate as a function of chemical potential at zero temperature for different values of the tensor coupling, let us look into the temperature behavior of F_3 for a fixed value of $G_T = 2g$. The temperature behavior of spin polarization condensate as well as σ_s is shown in Fig. 5. Figure 5 shows the contour plots of the thermodynamic potential in the plane of $\sigma_s - F_3$ for different values of temperature and chemical potential. Each row shows the behavior of the thermodynamic potential as a function of increasing chemical potential for a fixed temperature. On the other hand, each column shows the behavior of the thermodynamic potential as a function of temperature for a fixed value of chemical potential. From the first two rows in Fig. 5, for temperature $T = 0.02$ GeV and 0.04 GeV, it is

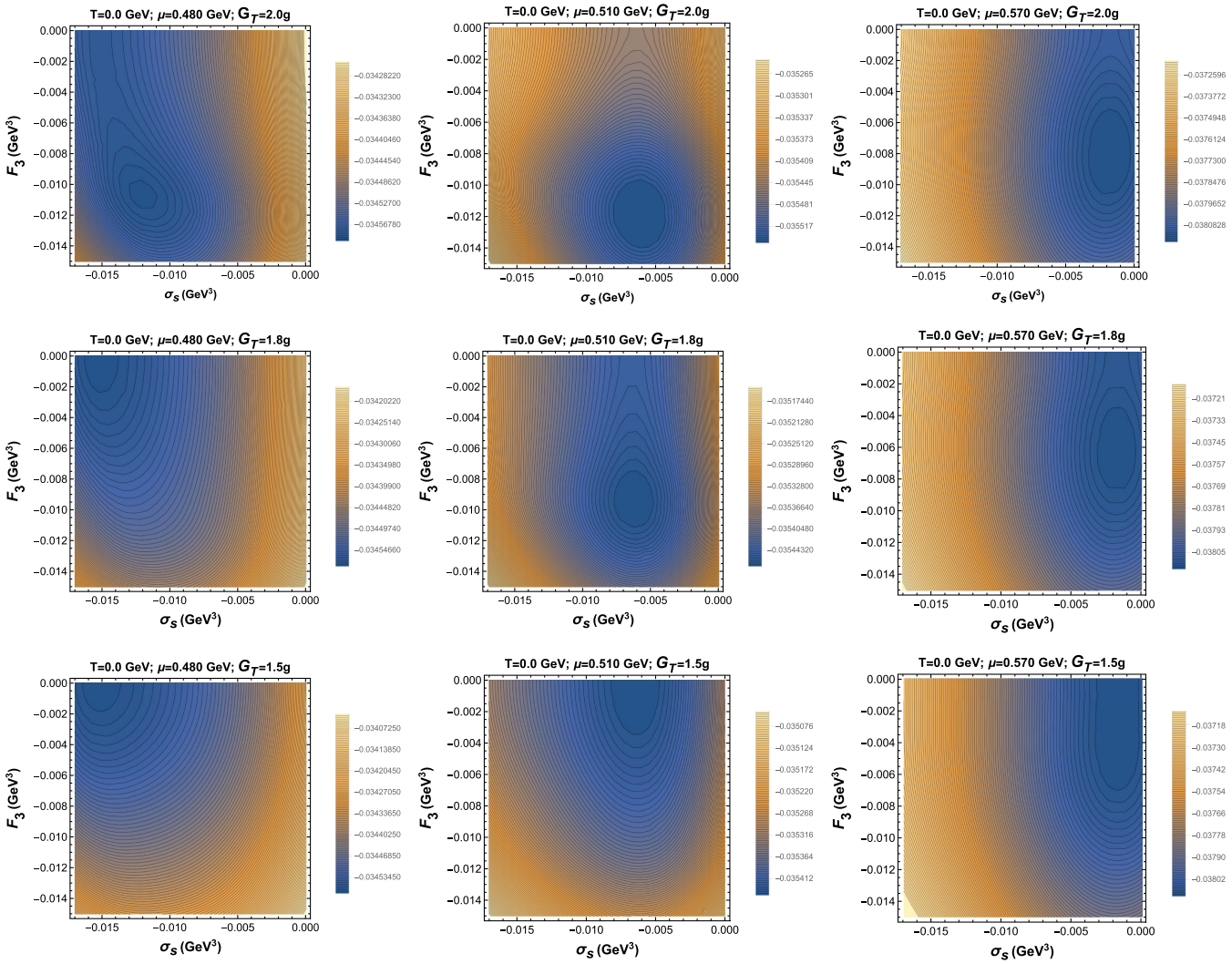

FIG. 6. This figure shows the contour plots of the thermodynamic potential in the $\sigma_s - F_3$ plane for zero temperature (T) and finite chemical potential (μ) with different values of tensor coupling G_T and $F_8 = F_3/\sqrt{3}$. In the first, second, and third rows, the tensor couplings are taken as $G_T = 2g$, $1.8g$, and $1.5g$, respectively. Along each row, the temperature and G_T have been kept fixed, but μ is increasing; similarly, along each column, μ and T have been kept fixed with G_T decreasing. Darker regions in these contour plots show the global minimum of the thermodynamic potential. It is clear from the plots that at zero temperature, for a larger value of tensor coupling, spin polarization can exist for a relatively wide range of chemical potential. With the decreasing value of tensor coupling, e.g., for $G_T = 1.5g$, spin polarization almost vanishes. This result can be easily extended to finite temperature. For nonzero temperature, the existence of spin polarization requires a larger value of G_T.

clear that as the chemical potential increases the nonzero value of spin polarization develops. It attains a maximum value at an intermediate value of the chemical potential, and as the chemical potential becomes very high, F_3 becomes zero. However, each column shows that with increasing temperature the formation of the spin polarization becomes difficult and the maximum value of F_3 also decreases with temperature. The third row in Fig. 5 shows that when the temperature is $T = 0.06$ GeV the value of the spin polarization condensate F_3 is almost zero. Hence, one can conclude that as the temperature increases the range of chemical potential within which spin polarization can exist decreases. Further, there exists a temperature beyond which spin polarization cannot occur irrespective of the value of chemical potential for a given value of G_T. Also note that with an increase in temperature and chemical potential the strange quark condensate (σ_s) decreases.

5. Threshold coupling for existence of F_3

The existence of spin polarization inevitably depends on the value of G_T. G_T determines the strength of the spin polarization condensation. The dependence of F_3 on the tensor coupling has been shown in Fig. 6. Figure 6 shows the thermodynamic potential in the $\sigma_s - F_3$ plane as a function of chemical potential for three different values of tensor couplings $G_T = 2g, 1.8g$, and $1.5g$ at zero temperature. Along each row in Fig. 6 the contours of thermodynamic potential have been shown for different values of the chemical potential but keeping G_T fixed. On the other hand, in each column of Fig. 6, contours of thermodynamic potential have been shown for various values the tensor coupling constant G_T for a given chemical potential. The value of the spin polarization condensate decreases with a decreasing value of G_T. When $G_T = 2g$, F_3 has a substantial nonzero value at zero temperature and

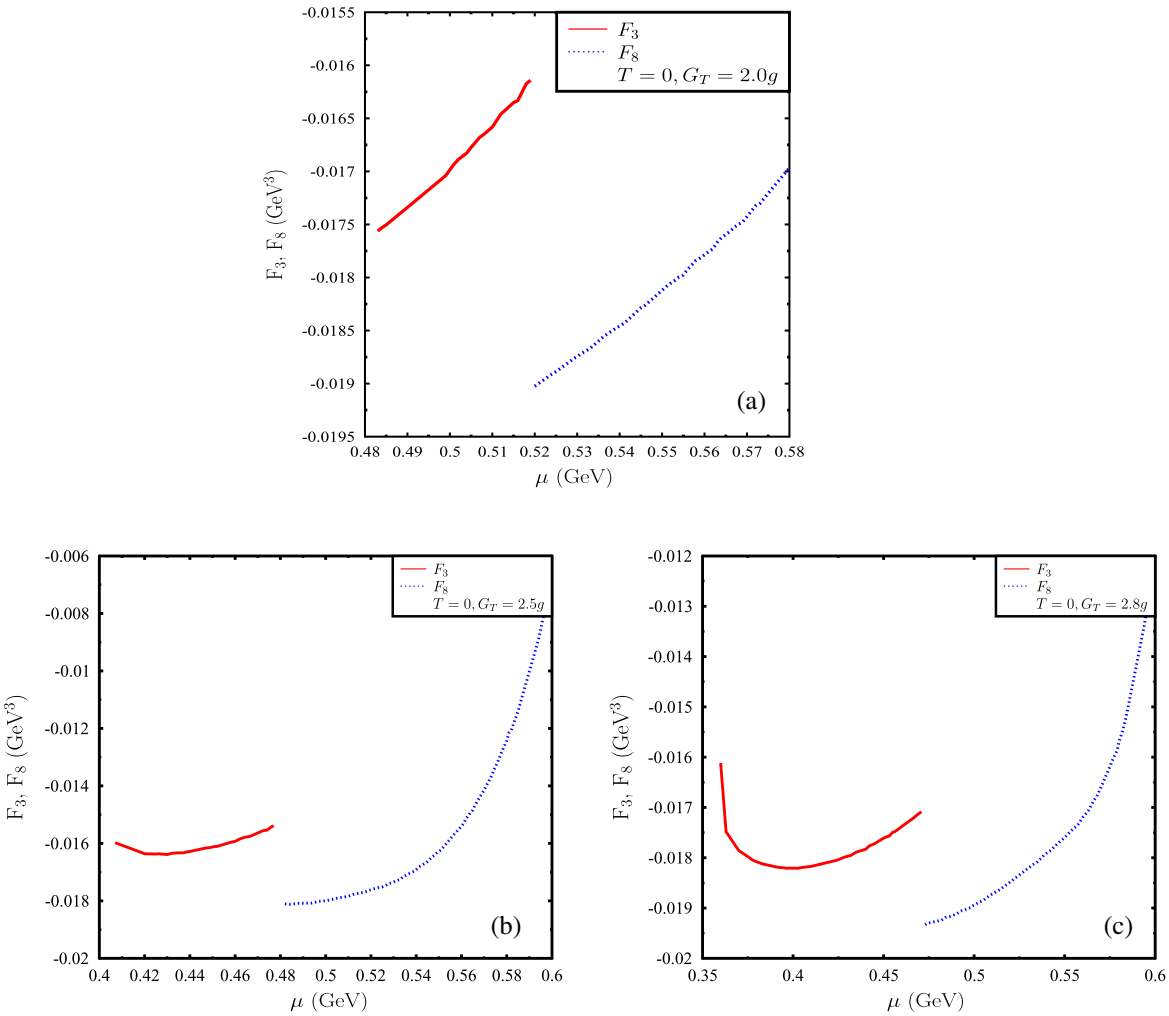

FIG. 7. Plots (a), (b), and (c) show the variation of F_3 (red solid line) and F_8 (blue dotted line) with chemical potential where F_3 and F_8 are considered simultaneously in the thermodynamic potential at zero temperature for $G_T = 2g$, $2.5g$, $2.8g$, respectively. It is clear from the Fig. 7 that nonzero F_3 appears at a relatively smaller μ than F_8. Since F_8 is associated with a strange quark-antiquark condensate, it survives even at larger chemical potential relative to the F_3 condensate. It is also important to notice that with a larger tensor coupling spin condensates appear at a relatively smaller quark chemical potential.

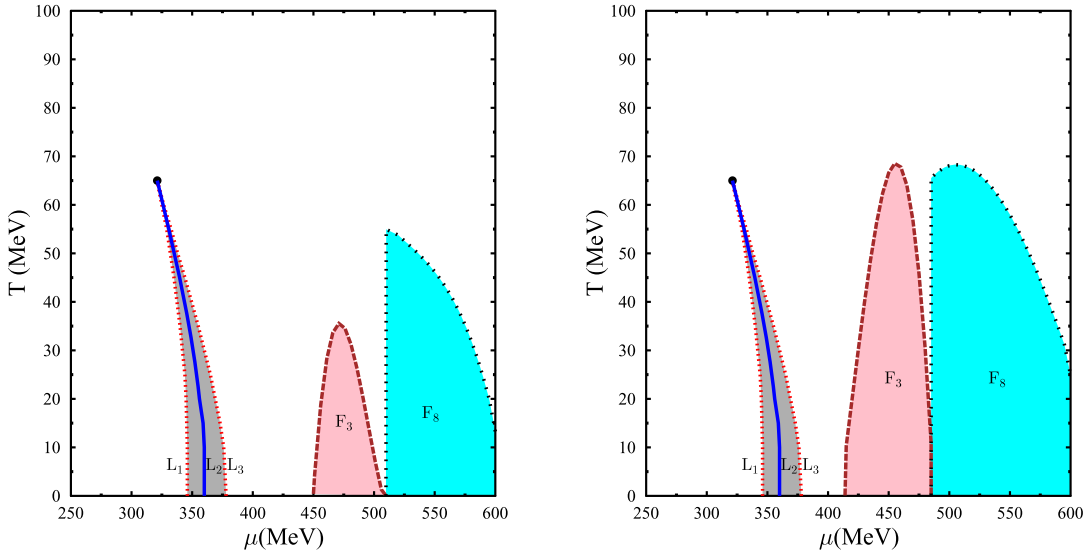

FIG. 8. Phase diagram for $G_T = 2g$ (left plot) and $G_T = 2.2g$ (right plot). The line L_2 corresponds to a first-order chiral phase transition. The lines L_1 and L_3 are the lower and upper spinodal lines. The pink shaded region corresponds to the region of μ and T where, the condensate F_3 is nonvanishing and $F_8 = 0$. The cyan shaded region is the range of chemical potential and temperature where the condensate F_8 is nonvanishing while $F_3 = 0$ in this region.

$\mu = 0.510$ GeV; however, for $G_T = 1.8g$, this value starts to decrease, and for $G_T = 1.5g$, the spin polarization condensate F_3 almost vanishes. This result for zero temperature can be easily extended to a nonzero temperature. For finite temperature, one requires a larger value of G_T, for the spin polarization to exist. As G_T increases, the threshold μ above which F_3 starts becoming nonvanishing decreases, and the critical μ above which F_3 vanishes increases. Both these behaviors lead to a larger range of μ that supports a nonvanishing F_3 as G_T increases. Further, the magnitude of F_3 increases with G_T.

B. Results for independent F_3, F_8

We have already discussed the variation of F_3 and F_8 with chemical potential where we have considered $F_8 = F_3/\sqrt{3}$ in the thermodynamic potential. However, for a more general situation, we have to consider F_3 and F_8 simultaneously. In Figs. 7(a), 7(b), and 7(c), we have shown the variation of F_3 and F_8 with chemical potential at zero temperature for $G_T = 2g, 2.5g, 2.8g$, respectively. It is clear from Fig. 7 that nonzero F_3 appears at a relatively smaller μ than F_8. Since F_8 is associated with strange quark-antiquark condensate, it survives even at larger chemical potential relative to the F_3 condensate. It is also important to notice that with larger tensor coupling spin condensates appear at a relatively smaller quark chemical potential.

In Fig. 8, we have shown the qualitative phase diagram including the spin polarized condensate for two values of tensor coupling. The left plot of Fig. 8 shows the phase diagram for $G_T = 2g$, while the right plot shows the same for $G_T = 2.2g$. For these values of tensor coupling, the chiral transition is unaffected even in the presence of spin polarized condensates. At low chemical potential, the chiral transition is a smooth crossover. At $\mu \sim 320$ MeV and $T \sim 65$ MeV, the chiral transition changes from a smooth crossover to first-order phase transition (as shown by the thick solid line in Fig. 8).

In Fig. 8, L_2 is the critical line in the phase diagram that separates the chiral symmetry broken and (almost) chiral symmetry restored phase. This first-order line ends at the critical point $(\mu_c, T_c) \sim (320, 65)$ MeV (denoted as a dot). The lines L_1 and L_3 are the lower and upper spinodal lines. The region between L_1 and L_2 has solutions for the gap equation with $\sigma_{ud} \simeq 0$ but has higher thermodynamical potential. Similarly, the region between L_3 and L_2 has a solution for gap equations with σ_{ud} having a large nonvanishing value, but with higher thermodynamic potential indicating metastable phases as seen in first-order phase transition.

Spin polarized condensates appear only at higher chemical potential in the chirally restored phase. In both the phase diagrams of Fig. 8, the region marked by F_3 corresponds to the phase where $F_3 \neq 0$ and $F_8 = 0$. The region marked by F_8 corresponds to the phase where $F_8 \neq 0$ while $F_3 = 0$. We find that the phase with simultaneous $F_3 \neq 0$ and $F_8 \neq 0$ is not the thermodynamically favored ground state. For $G_T = 2g$, the F_3 condensate appears at $\mu \sim 450$ MeV. At $\mu \sim 510$ MeV, the $F_8 \neq 0$ state becomes favored compared to the $F_3 \neq 0$ state. As the temperature increases, the magnitude of F_3 and F_8 decreases, and beyond a certain critical temperature, the condensates vanish. The critical temperature for the spin polarized condensates shows a nonmonototic behavior with quark chemical potential. For the F_3 condensate, the maximum critical temperature turns out to be $T \sim 35$ MeV, and for the F_8 condensate,

the same happens at $T \sim 55$ MeV for chemical potentials $\mu \sim 470$ MeV and $\mu \sim 510$ MeV, respectively. For $G_T = 2.2g$, the F_3 condensate appears at $\mu \sim 415$ MeV as a result of higher tensor coupling. The $F_8 \neq 0$ state becomes favored at $\mu \sim 485$ MeV. Compared to $G_T = 2g$, the magnitudes of F_3 and F_8 condensates are larger in this case. Further, it is observed that the maximum critical temperature for both the spin polarized condensates F_3 and F_8 is $T \sim 68$ MeV for chemical potential $\mu \sim 455$ MeV and $\mu \sim 505$ MeV, respectively.

We would like to comment here that in the present investigation we have not included the diquark condensate. The simultaneous existence of F_3 and the color superconducting phase was shown earlier [39].

The spin polarization condensate implies an alignment of the spin of quarks. This will lead to a magnetic field due to the quark magnetic moment. We estimate the strength of the effective magnetic field (B_{eff}) due to the spin polarization condensate as [35]

$$\bar{\mu}_q B_{\text{eff}} = G_T F, \qquad \bar{\mu}_q = \frac{\mu_u + \mu_d}{2},$$
$$\bar{\mu}_u = \frac{(\frac{2}{3}e)}{2m_q}, \qquad \bar{\mu}_d = \frac{(-\frac{1}{3}e)}{2m_q}. \tag{13}$$

Here, F denotes the spin polarization condensate, and $\bar{\mu}_q$ is the average magnetic moment of the light quarks. For an estimation of B_{eff}, we take $F \sim 0.018$ GeV^3 (at quark chemical potential approximately 510 MeV) and $G_T = 2g$. Using these values, we get $eB_{\text{eff}} \sim m_\pi^2$ or 10^{18} G. The value of the magnetic field on the surface of the magnetars is of the order of 10^{15} G, but in the center, the strength of the magnetic field can be higher. It is interesting to note that even this crude estimation of the magnetic field due to the spin polarized phase of the deconfined quark matter leads to a correct order of magnitude estimation of the magnetic field in the core of the magnetars.

IV. CONCLUSIONS

In this work, we have considered the $(2+1)$-flavor NJL model in the presence of tensor interaction with nonzero current quark masses. The original idea of the presence of spin polarization in quark liquid was motivated considering one-gluon-exchange interactions in perturbative QCD processes [28]. Ferromagnetic quark matter can arise due to both axial vector–type and tensor-type interaction. Although the axial vector–type interaction can be generated from the one-gluon-exchange QCD interaction by Fierz transformation, the tensor-type interactions cannot be generated using Fierz transformation. Thus, at very high densities at which the perturbative QCD processes are relevant, the tensor type of interaction will not be suitable to study spin polarization in quark matter. More importantly, at moderate densities, close to the chiral phase transition, one expects nonperturbative effects to play an important role. In the present investigation within the ambit of the NJL model applied to moderate densities, we have considered only the tensor-type four-point interaction. We might note here that the coupling constant of the tensor interaction is related to the scalar and pseudoscalar channels. However, in general, this tensor coupling constant can be independent. We take the coupling constant of the tensor interaction G_T as a parameter of the model. We have taken various values of the tensor couplings G_T, e.g., $G_T = 2.0g$ and lower, as well as relatively larger values of G_T, e.g., $G_T = 2.5g$, $2.8g$, etc.

For the $(2+1)$-flavor NJL model, tensor-type interaction at the mean field level leads to two types of spin polarization condensates, $F_3 = \langle\bar{\psi}\Sigma_z\lambda_3\psi\rangle$ and $F_8 = \langle\bar{\psi}\Sigma_z\lambda_8\psi\rangle$. Since we have various condensates in the $(2+1)$-flavor NJL model in the presence of tensor interaction, we take a somewhat simplified approximation, in which F_3 and F_8 are not independent but rather $F_8 = F_3/\sqrt{3}$. This oversimplification corresponds to treating down quarks on equal footing with strange quarks, which probably can be a reasonable approximation in asymptotic densities at which one may neglect the quark masses compared to the chemical potentials. In fact, treating F_3 and F_8 independently, for moderate densities, it is shown that the nonstrange spin polarization condensate F_3 and the one including the strange quarks F_8 do not coexist. One may note that, in general, F_3 and F_8 are independent due to the fact that F_8 is associated with the strange quark spin polarization condensate; on the other hand, F_3 contains only u and d quark spin polarization condensates. Therefore, we have also considered the case in which F_3 and F_8 are treated independently. Generically, spin polarization for moderate tensor coupling (e.g., $G_T = 2g$) does not appear at zero temperature and zero chemical potential; rather, it appears at high μ in the chiral restored phase. At large chemical potential and small temperature, the generic feature of such a spin polarized condensate lies in affecting the strange quark mass rather than the nonstrange quark masses for moderate tensor coupling. Such a spin polarized condensate vanishes for temperatures of the order of few tens of MeV and thus can be relevant for neutron stars and protoneutron stars. However, it ought to be investigated whether such conclusion holds well when charge neutrality conditions on the bulk matter are imposed. We also find that there is a threshold for the tensor coupling, below which the spin polarization condensates do not develop.

Unlike the superconducting diquark condensate, the spin polarization condensate is not a monotonic function of chemical potential, and as the chemical potential is increased, the magnitude becomes a maximum beyond which it vanishes when μ is increased further. The range of chemical potential for which such a condensate exists, as well as the magnitude of the condensate, increases with the strength of the tensor coupling. We estimate the magnitude of the magnetic field corresponding to the ferromagnetic condensate in high-density quark matter to be of the order

of approximately $m_\pi^2 \sim 10^{18}$ G. It is important to mention that, although the spin polarization condensate was thought as a source of magnetic field in magnetars, magnetic field can also be present in the neutron stars originated from the progenitor star. External magnetic field can affect the formation of spin condensates. In this context, it has been shown recently that one can have a nonvanishing spin polarization condensate for quark matter in the presence of magnetic field [55].

In this exploratory study, we have tried to investigate the possibility of phase transition of dense quark matter to a spin polarized phase of quark matter within a phenomenological $(2+1)$-flavor Nambu–Jona-Lasinio model with the tensor coupling being a free parameter. However, applying it to a physical situation like compact stars requires a careful consideration of possible other phases of dense matter like, e.g., color superconductivity, the imposition of charge neutrality conditions for bulk matter.

ACKNOWLEDGMENTS

We would like to thank Robert Pisarski for important comments on this work. R. K. M. would like to thank Theoretical Physics Division of Physical Research Laboratory, Ahmedabad, for support and local hospitality for her visit, during which this problem was initiated. Also R. K. M. would like to thank Basanta K. Nandi and Sadhana Dash for constant support and encouragement.

APPENDIX

The gap equations for four independent condensates, two chiral condensates σ_{ud} and σ_s, and two spin polarization condensates F_3 and F_8 are as follows:

$$\begin{aligned}\frac{\partial\Omega}{\partial\sigma_{ud}} = -N_c\int\frac{d^3p}{(2\pi)^3}\Bigg[&\frac{M_u}{E_{u_+}}\left(1+\frac{G_T(F_3+F_8/\sqrt{3})}{\sqrt{p_T^2+M_u^2}}\right)(-4g+2K\sigma_s)\left\{1-\frac{1}{1+e^{\beta(E_{u_+}-\mu)}}-\frac{1}{1+e^{\beta(E_{u_+}+\mu)}}\right\}\\
&+\frac{M_u}{E_{u_-}}\left(1-\frac{G_T(F_3+F_8/\sqrt{3})}{\sqrt{p_T^2+M_u^2}}\right)(-4g+2K\sigma_s)\left\{1-\frac{1}{1+e^{\beta(E_{u_-}-\mu)}}-\frac{1}{1+e^{\beta(E_{u_-}+\mu)}}\right\}\\
&+\frac{M_d}{E_{d_+}}\left(1+\frac{G_T(F_3-F_8/\sqrt{3})}{\sqrt{p_T^2+M_d^2}}\right)(-4g+2K\sigma_s)\left\{1-\frac{1}{1+e^{\beta(E_{d_+}-\mu)}}-\frac{1}{1+e^{\beta(E_{d_+}+\mu)}}\right\}\\
&+\frac{M_d}{E_{d_-}}\left(1-\frac{G_T(F_3-F_8/\sqrt{3})}{\sqrt{p_T^2+M_d^2}}\right)(-4g+2K\sigma_s)\left\{1-\frac{1}{1+e^{\beta(E_{d_-}-\mu)}}-\frac{1}{1+e^{\beta(E_{d_-}+\mu)}}\right\}\\
&+\frac{M_s}{E_{s_+}}\left(1+\frac{2G_TF_8/\sqrt{3}}{\sqrt{p_T^2+M_s^2}}\right)(4K\sigma_{ud})\left\{1-\frac{1}{1+e^{\beta(E_{s_+}-\mu)}}-\frac{1}{1+e^{\beta(E_{s_+}+\mu)}}\right\}\\
&+\frac{M_s}{E_{s_-}}\left(1-\frac{2G_TF_8/\sqrt{3}}{\sqrt{p_T^2+M_s^2}}\right)(4K\sigma_{ud})\left\{1-\frac{1}{1+e^{\beta(E_{s_-}-\mu)}}-\frac{1}{1+e^{\beta(E_{s_-}+\mu)}}\right\}\Bigg]+8g\sigma_{ud}-8K\sigma_{ud}\sigma_s=0\end{aligned}\tag{A1}$$

$$\begin{aligned}\frac{\partial\Omega}{\partial\sigma_s} = -N_c\int\frac{d^3p}{(2\pi)^3}\Bigg[&\frac{M_u}{E_{u_+}}\left(1+\frac{G_T(F_3+F_8/\sqrt{3})}{\sqrt{p_T^2+M_u^2}}\right)(2K\sigma_{ud})\left\{1-\frac{1}{1+e^{\beta(E_{u_+}-\mu)}}-\frac{1}{1+e^{\beta(E_{u_+}+\mu)}}\right\}\\
&+\frac{M_u}{E_{u_-}}\left(1-\frac{G_T(F_3+F_8/\sqrt{3})}{\sqrt{p_T^2+M_u^2}}\right)(2K\sigma_{ud})\left\{1-\frac{1}{1+e^{\beta(E_{u_-}-\mu)}}-\frac{1}{1+e^{\beta(E_{u_-}+\mu)}}\right\}\\
&+\frac{M_d}{E_{d_+}}\left(1+\frac{G_T(F_3-F_8/\sqrt{3})}{\sqrt{p_T^2+M_d^2}}\right)(2K\sigma_{ud})\left\{1-\frac{1}{1+e^{\beta(E_{d_+}-\mu)}}-\frac{1}{1+e^{\beta(E_{d_+}+\mu)}}\right\}\\
&+\frac{M_d}{E_{d_-}}\left(1-\frac{G_T(F_3-F_8/\sqrt{3})}{\sqrt{p_T^2+M_d^2}}\right)(2K\sigma_{ud})\left\{1-\frac{1}{1+e^{\beta(E_{d_-}-\mu)}}-\frac{1}{1+e^{\beta(E_{d_-}+\mu)}}\right\}\\
&+\frac{M_s}{E_{s_+}}\left(1+\frac{2G_TF_8/\sqrt{3}}{\sqrt{p_T^2+M_s^2}}\right)(-4g)\left\{1-\frac{1}{1+e^{\beta(E_{s_+}-\mu)}}-\frac{1}{1+e^{\beta(E_{s_+}+\mu)}}\right\}\\
&+\frac{M_s}{E_{s_-}}\left(1-\frac{2G_TF_8/\sqrt{3}}{\sqrt{p_T^2+M_s^2}}\right)(-4g)\left\{1-\frac{1}{1+e^{\beta(E_{s_-}-\mu)}}-\frac{1}{1+e^{\beta(E_{s_-}+\mu)}}\right\}\Bigg]+4g\sigma_s-4K\sigma_{ud}^2=0\end{aligned}\tag{A2}$$

$$\frac{\partial\Omega}{\partial F_3} = -N_c \int \frac{d^3p}{(2\pi)^3}\left[G_T\frac{\sqrt{p_T^2+M_u^2}+G_T(F_3+F_8/\sqrt{3})}{E_{u_+}}\left\{1-\frac{1}{1+e^{\beta(E_{u_+}-\mu)}}-\frac{1}{1+e^{\beta(E_{u_+}+\mu)}}\right\}\right.$$
$$-G_T\frac{\sqrt{p_T^2+M_u^2}-G_T(F_3+F_8/\sqrt{3})}{E_{u_-}}\left\{1-\frac{1}{1+e^{\beta(E_{u_-}-\mu)}}-\frac{1}{1+e^{\beta(E_{u_-}+\mu)}}\right\}$$
$$+G_T\frac{\sqrt{p_T^2+M_d^2}+G_T(F_3-F_8/\sqrt{3})}{E_{d_+}}\left\{1-\frac{1}{1+e^{\beta(E_{d_+}-\mu)}}-\frac{1}{1+e^{\beta(E_{d_+}+\mu)}}\right\}$$
$$\left.-G_T\frac{\sqrt{p_T^2+M_d^2}-G_T(F_3-F_8/\sqrt{3})}{E_{d_-}}\left\{1-\frac{1}{1+e^{\beta(E_{d_-}-\mu)}}-\frac{1}{1+e^{\beta(E_{d_-}+\mu)}}\right\}\right]+G_TF_3=0 \tag{A3}$$

$$\frac{\partial\Omega}{\partial F_8} = -N_c \int \frac{d^3p}{(2\pi)^3}\left[\frac{G_T}{\sqrt{3}}\frac{\sqrt{p^2+M_u^2}+G_T(F_3+F_8/\sqrt{3})}{E_{u_+}}\left\{1-\frac{1}{1+e^{\beta(E_{u_+}-\mu)}}-\frac{1}{1+e^{\beta(E_{u_+}+\mu)}}\right\}\right.$$
$$-\frac{G_T}{\sqrt{3}}\frac{\sqrt{p^2+M_u^2}-G_T(F_3+F_8/\sqrt{3})}{E_{u_-}}\left\{1-\frac{1}{1+e^{\beta(E_{u_-}-\mu)}}-\frac{1}{1+e^{\beta(E_{u_-}+\mu)}}\right\}$$
$$-\frac{G_T}{\sqrt{3}}\frac{\sqrt{p^2+M_d^2}+G_T(F_3-F_8/\sqrt{3})}{E_{d_+}}\left\{1-\frac{1}{1+e^{\beta(E_{d_+}-\mu)}}-\frac{1}{1+e^{\beta(E_{d_+}+\mu)}}\right\}$$
$$+\frac{G_T}{\sqrt{3}}\frac{\sqrt{p^2+M_d^2}-G_T(F_3-F_8/\sqrt{3})}{E_{d_-}}\left\{1-\frac{1}{1+e^{\beta(E_{d_-}-\mu)}}-\frac{1}{1+e^{\beta(E_{d_-}+\mu)}}\right\}$$
$$+2\frac{G_T}{\sqrt{3}}\frac{\sqrt{p^2+M_s^2}+2G_TF_8/\sqrt{3}}{E_{s_+}}\left\{1-\frac{1}{1+e^{\beta(E_{s_+}-\mu)}}-\frac{1}{1+e^{\beta(E_{s_+}+\mu)}}\right\}$$
$$\left.-2\frac{G_T}{\sqrt{3}}\frac{\sqrt{p^2+M_s^2}-2G_TF_8/\sqrt{3}}{E_{s_-}}\left\{1-\frac{1}{1+e^{\beta(E_{s_-}-\mu)}}-\frac{1}{1+e^{\beta(E_{s_-}+\mu)}}\right\}\right]+G_TF_8=0. \tag{A4}$$

[1] D. H. Rischke, Prog. Part. Nucl. Phys. **52**, 197 (2004).
[2] K. Rajagopal and F. Wilczek, in *At the Frontier of Particle Physics*, edited by M. Shifman (World Scientific, Singapore, 2001), Vol. 3, pp. 2061–2151.
[3] F. Karsch, Lect. Notes. Phys. **583**, 209 (2002).
[4] E. Laerman and O. Philipsen, Annu. Rev. Nucl. Part. Sci. **53**, 163 (2003).
[5] M. Cheng *et al.*, Phys. Rev. D **77**, 014511 (2008).
[6] Z. Foder and S. Katz, J. High Energy Phys. 03 (2002) 014; Ph. de Forcrand and O. Phillipsen, Nucl. Phys. **B642**, 290 (2002); M. D'Elia and M. P. Lombardo, Phys. Rev. D **67**, 014505 (2003); C. R. Allton, S. Ejiri, S. J. Hands, O. Kaczmarek, F. Karsch, E. Laermann, Ch. Schmidt, and L. Scorzato, Phys. Rev. D **66**, 074507 (2002); C. R. Allton, S. Ejiri, S. J. Hands, O. Kaczmarek, F. Karsch, E. Laermann, and C. Schmidt, Phys. Rev. D **68**, 014507 (2003).
[7] H. T. Ding, Nucl. Phys. **A931**, 52 (2014).
[8] M. G. Alford, A. Schmitt, K. Rajagopal, and T. Schafer, Rev. Mod. Phys. **80**, 1455 (2008), and references therein.
[9] M. Alford, K. Rajagopal, and F. Wilczek, Nucl. Phys. **B537**, 443 (1999).
[10] K. Iida and G. Byam, Phys. Rev. D **63**, 074018 (2001).
[11] L. McLerran and R. D. Pisarski, Nucl. Phys. **A796**, 83 (2007).
[12] E. Nakano and T. Tatsumi, Phys. Rev. D **71**, 114006 (2005).
[13] D. Nickel, Phys. Rev. Lett. **103**, 072301 (2009).
[14] M. Buballa and S. Carignano, Prog. Part. Nucl. Phys. **81**, 39 (2015), and references therein.
[15] G. Baym, T. Hatsuda, T. Kojo, P. D. Powell, Y. Song, and T. Takatsuka, Rep. Prog. Phys. **81**, 056902 (2018).
[16] N. Itoh, Prog. Theor. Phys. **44**, 291 (1970).
[17] T. Kunihiro, T. Takatsuka, R. Tamagaki, and T. Tatsumi, Prog. Theor. Phys. Suppl. **112**, 123 (1993).

[18] D. Bandyopadhyaya, S. Chakrabarty, and S. Pal, Phys. Rev. Lett. **79**, 2176 (1997); S. Chakrabarty and S. Mandal, Phys. Rev. C **75**, 015805 (2007).
[19] R. C. Duncan and C. Thompson, Astrophys. J. **392**, L9 (1992).
[20] C. Thompson and R. C. Duncan, Astrophys. J. **408**, 194 (1993).
[21] C. Thompson and R. C. Duncan, Mon. Not. R. Astron. Soc. **275**, 255 (1995).
[22] C. Thompson and R. C. Duncan, Astrophys. J. **473**, 322 (1996).
[23] C. Y. Cardall, M. Prakash, and J. M. Lattimer, Astrophys. J. **554**, 322 (2001).
[24] A. E. Broderick, M. Prakash, and J. M. Lattimer, Phys. Lett. B **531**, 167 (2002).
[25] D. Lai and S. L. Shapiro, Astrophys. J. **383**, 745 (1991).
[26] E. J. Ferrer, V. Incera, J. P. Keith, I. Portillo, and P. Springsteen, Phys. Rev. C **82**, 065802 (2010).
[27] G. Chanmugam, Annu. Rev. Astron. Astrophys. **30**, 143 (1992).
[28] T. Tatsumi, Phys. Lett. B **489**, 280 (2000).
[29] T. Maruyama and T. Tatsumi, Nucl. Phys. **A693**, 710 (2001).
[30] E. Nakano, T. Maruyama, and T. Tatsumi, Phys. Rev. D **68**, 105001 (2003).
[31] V. R. Pandharipande, V. K. Garde, and J. K. Srivastava, Phys. Lett. **38B**, 485 (1972).
[32] R. Niembro, S. Marcos, M. L. Quelle, and J. Navarro, Phys. Lett. B **249**, 373 (1990).
[33] S. Marcos, R. Niembro, and M. L. Quelle, Phys. Lett. B **271**, 277 (1991).
[34] S. Maedan, Prog. Theor. Phys. **118**, 729 (2007).
[35] Y. Tsue, J. de. Providencia, C. Providencia, and M. Yamamura, Prog. Theor. Phys. **128**, 507 (2012).
[36] T. Maruyama, E. Nakano, and T. Tatsumi, *Horizons in World Physics* (Nova Science, New York, 2011), Vol. 276, Chap. 7.
[37] Y. Tsue, J. de. Providencia, C. Providencia, M. Yamamura, and H. Bohr, Prog. Theor. Exp. Phys. **2015**, 103D01 (2015).
[38] Y. Tsue, J. Providência, C. Providência, M. Yamamura, and H. Bohr, Prog. Theor. Exp. Phys. **103**, D02 (2015).
[39] H. Matsuoka, Y. Tsue, J. da Providencia, C. Providencia, and M. Yamamura, Phys. Rev. D **95**, 054025 (2017).
[40] H. Matsuoka, Y. Tsue, J. da Providencia, C. Providencia, M. Yamamura, and H. Bohr, Prog. Theor. Exp. Phys. **2016**, 053D02 (2016).
[41] M. Morimoto, Y. Tsue, J. da Providencia, C. Providencia, and Y. Yamamura, Int. J. Mod. Phys. E **27**, 1850028 (2018).
[42] H. Bohr, P. K. Panda, C. Providencia, and J. D. Providencia, Int. J. Mod. Phys. E **22**, 1350019 (2013).
[43] M. Buballa, Phys. Rep. **407**, 205 (2005).
[44] U. Vogl and W. Weise, Prog. Part. Nucl. Phys. **27**, 195 (1991).
[45] T. Hatsuda and T. Kunihiro, Phys. Rep. **247**, 221 (1994).
[46] P. Rehberg, S. P. Klevansky, and J. Hufner, Phys. Rev. C **53**, 410 (1996).
[47] S. P. Klevansky, Rev. Mod. Phys. **64**, 649 (1992).
[48] H. Kohyama, D. Kimura, and T. Inagaki, Nucl. Phys. **B906**, 524 (2016).
[49] H. Kohyama, D. Kimura, and T. Inagaki, Nucl. Phys. **B896**, 682 (2015).
[50] M. Jaminon and E. Ruiz Arriola, Phys. Lett. B **443**, 33 (1998).
[51] M. Jaminon, M. C. Ruvio, and C. A. de Sousa, Int. J. Mod. Phys. A **17**, 4903 (2002).
[52] O. A. Battistel, T. H. Pimenta, and G. Dallabona, Phys. Rev. D **94**, 085011 (2016).
[53] M. Lutz, S. Klimt, and W. Weise, Nucl. Phys. **A542**, 521 (1992).
[54] P. Rehberg, S. P. Klevansky, and J. Huefner, Phys. Rev. C **53**, 410 (1996).
[55] S. Mao and D. H. Rischke, Phys. Lett. B **792**, 149 (2019).